

Crossing symmetry and scaling properties of pp and p \bar{p} forward scattering amplitudes

A. K. Kohara*

CPHT, CNRS, Ecole polytechnique, IP Paris, F-91128 Palaiseau, France

Abstract

We analyse the pp and p \bar{p} elastic scattering amplitudes using the data of several CERN and FERMILAB experiments, revisiting ideas proposed by André Martin based on analytic continuation and crossing symmetry. Introducing a new form for the scaling function together with the analytical forms from COMPETE at $t = 0$ we show that the data are consistent with the crossing symmetry of the scattering amplitudes from $\sqrt{s} = 23$ GeV to 13 TeV for $-t \leq 0.2$ GeV². Analyticity and crossing symmetry automatically satisfy the dispersion relations and their derivatives. The real part reproduces the zero predicted by Martin, which is crucial to describe with precision the differential cross section in the forward range at high energies. Since the free parameters of the model are energy independent, the analytical form of the amplitude allows predictions for intermediate and higher energies.

Keywords: elastic scattering amplitudes, analyticity, crossing symmetry, dispersion relations, scaling, total cross section

Theoretical and phenomenological approaches for the description of pp and p \bar{p} elastic scattering aim to determine the dynamics and kinematical dependence of the amplitudes, described in terms of the two variables s and t . In Regge theory the rise of the hadronic total cross section can be described by
 5 the Pomeron trajectory linear in t , with power dependence on s in the case of

*Corresponding author

Email address: `kendi@if.ufrj.br` (A. K. Kohara)

a simple pole. However at high energies the growth of the total cross section guided by the Froissart bound [1] and by the behaviour of the observed data can be parametrized as a quadratic form in $\log(s/s_0)$ such as $\sigma \sim \log^2(s/s_0)$, where we consider $s_0 = 1$ GeV, and we omit s_0 for simplicity. The form of
10 the differential cross section depends on specific assumptions for the real and imaginary amplitudes, controlled by dispersion relations (DR). In what follows we use the variable $E = (s - u)/4m$ as a crossing symmetric variable, which coincides with the energy in the laboratory frame for $t = 0$.

In another treatment for very large energies in the forward region, if the
15 real amplitude is neglected compared with the imaginary part, the scattering amplitude $F^N(E, t)$ is suggested to follow a scaling dependence [2], with $F^N(E, t)/F^N(E, 0) = f(\tau)$ where τ is a combination of E and t variables. Using the $\log^2(E)$ dependence combined with the scaling function $f(\tau)$ the scattering amplitude is then written with the form,

$$F^N(E, t) \sim i C E \log^2(E) f(\tau) . \quad (1)$$

20 The bounds and constraints of $f(\tau)$ were formally studied long ago [2] in the context of axiomatic field theory, giving $f(\tau) \leq \kappa \exp(\sqrt{|\tau|})$, where κ is constant and the scaling variable is $\tau = t \log^2 E$. The cross section corresponding to Eq.(1) is not invariant under the transformation, $E \rightarrow -E$ (crossing symmetry). Following A. Martin [3], in order to define a complex crossing symmetric
25 function, Eq.(1) can be modified to

$$F^N(E, t) \sim i C E \left(\log(E) - i \frac{\pi}{2} \right)^2 f(\tau') . \quad (2)$$

The extension of $\log(E)$ in the complex plane changes the scaling variable to a complex variable $\tau' = t [\log(E) - i\pi/2]^2$ which transforms the scaling function $f(\tau')$ in a complex quantity.

However, it is not obvious that at large energies these amplitudes, with both
30 crossing and scaling, are well satisfied. Attempts have been made in this direction to analyse ISR energies with $f(s, t) = \sum_{i=1}^n a_i e^{b_i t}$ where a_i and b_i are free parameters to be fitted at each energy [4]. To test the ideas of crossing and

scaling we propose in the current work a modified model for the forward scattering at high energies using the analytical crossing symmetric forms explored
 35 by Block and Cahn [5] and used in the COMPETE parametrization [6], and writing¹

$$\mathcal{R}_+(E, \alpha) = 2 E^\alpha \cos(\alpha \beta) \exp(-i \alpha \beta) \quad (3)$$

$$\mathcal{C}_+(E) = i E \quad (4)$$

$$\mathcal{L}_+(E) = \log(E) - i \beta \quad (5)$$

$$\mathcal{R}_-(E, \alpha) = 2 i E^\alpha \sin(\alpha \beta) \exp(-i \alpha \beta) . \quad (6)$$

Crossing symmetry imposes $\beta = \pi/2$, but here we let β free for a test against the data. The subscripts (+) and (-) refer to even and odd terms under crossing symmetry. We generalize Eq.(2) writing

$$F_{\mp}^N(E, t) = \mathcal{C}_+(E) \left[P' + P'_1 \mathcal{L}_+(E) + H' (\mathcal{L}_+(E))^2 + R'_1 \mathcal{R}_+(E, -\eta_1) \right. \\ \left. \mp R'_2 \mathcal{R}_-(E, -\eta_2) \right] f(\tau') , \quad (7)$$

40 where \mp are refereed to pp/p \bar{p} respectively. The parameters P' , P'_1 , H' , R'_1 , R'_2 , η'_1 and η'_2 are fixed numbers for all energies.

The t dependence is embedded in the complex scaling variable τ' defined as

$$\tau'(E, t) = \left[b'_0 + b'_1 \mathcal{L}_+(E) + b'_2 (\mathcal{L}_+(E))^2 + b'_3 \mathcal{R}_+(E, -\eta_3) \right] t , \quad (8)$$

with b'_0 , b'_1 , b'_2 , b'_3 as fixed quantities, while η'_3 is allowed to have energy dependence. We assume a complex scaling function

$$f(\tau') \equiv e^{\tau'} = e^{\Omega'_R(E, t) + i \Omega'_I(E, t)} . \quad (9)$$

45 Since we are interested in a high energy region we can approximate $s \approx 2 m E$ and we re-write the amplitudes using the s variable

$$F_{\mp}^N(s, t) = \left[F_{\mp}^R(s) + i F_{\mp}^I(s) \right] f(\tau') \\ = \left[F_{\mp}^R(s) + i F_{\mp}^I(s) \right] e^{\Omega_R(s, t) + i \Omega_I(s, t)} . \quad (10)$$

¹These analytical functions are written above the right hand cut in the complex E-plane.

Separating the real and imaginary parts we have

$$F_{\mp}^R(s) = s \left[\beta \left(P_1 + 2 H \log(s) \right) - R_1 s^{-\eta_1} \sin(\eta_1 \beta) \mp R_2 s^{-\eta_2} \cos(\eta_2 \beta) \right], \quad (11)$$

$$F_{\mp}^I(s) = s \left[P + P_1 \log(s) + H \left(\log^2(s) - \beta^2 \right) + R_1 s^{-\eta_1} \cos(\eta_1 \beta) \pm R_2 s^{-\eta_2} \sin(\eta_2 \beta) \right], \quad (12)$$

and

$$\Omega_R(s, t) = \left[b_0 + b_1 \log(s) + b_2 \left(\log^2(s) - \beta^2 \right) + b_3 s^{-\eta_3} \cos(\eta_3 \beta) \right] t, \quad (13)$$

50

$$\Omega_I(s, t) = - \left[b_1 \beta + 2 b_2 \beta \log(s) - b_3 s^{-\eta_3} \sin(\eta_3 \beta) \right] t. \quad (14)$$

We adopt the suggestion from COMPETE parametrization [6] for the amplitudes at $t = 0$ with the same given parameters P , P_1 , H , R_1 , R_2 , η_1 and η_2 , while β is left as a free parameter to test the crossing symmetry. The parameters that dictate the forward t dependence of the differential cross section are b_0 , b_1 ,
 55 b_2 , b_3 (energy independent) while the energy dependence of η_3 is obtained from differential cross section data.

The separation of the real and imaginary gives

$$F_{\mp}^R(s, t) = F_{\mp}^I(s) \left[-\sin \Omega_I(s, t) + \frac{F_{\mp}^R(s)}{F_{\mp}^I(s)} \cos \Omega_I(s, t) \right] e^{\Omega_R(s, t)} \quad (15)$$

and

$$F_{\mp}^I(s, t) = F_{\mp}^I(s) \left[\cos \Omega_I(s, t) + \frac{F_{\mp}^R(s)}{F_{\mp}^I(s)} \sin \Omega_I(s, t) \right] e^{\Omega_R(s, t)}. \quad (16)$$

The complex amplitude can be written in the compact form

$$\begin{pmatrix} F_{\mp}^R(s, t) \\ F_{\mp}^I(s, t) \end{pmatrix} = s \sigma_{\mp}(s) \begin{pmatrix} \cos \Omega_I(s, t) & -\sin \Omega_I(s, t) \\ \sin \Omega_I(s, t) & \cos \Omega_I(s, t) \end{pmatrix} \begin{pmatrix} \rho_{\mp}(s) \\ 1 \end{pmatrix} e^{\Omega_R(s, t)}, \quad (17)$$

60 where $\Omega_I(s, t)$ is the forward mixing angle between ρ_{\mp} and the unity. The total cross sections for $pp/p\bar{p}$ are given by the optical theorem

$$\sigma_{\mp}(s) = \frac{F_{\mp}^I(s, 0)}{s}, \quad (18)$$

and the ratios of the amplitudes at $-t = 0$ are

$$\rho_{\mp}(s) = \frac{F_{\mp}^R(s, 0)}{F_{\mp}^I(s, 0)} . \quad (19)$$

Note that Eq.(17) has trigonometric functions which make the sum of the absolute square of the real and imaginary nuclear parts as a simple exponential function

$$|F_{\mp}^R(s, t)|^2 + |F_{\mp}^I(s, t)|^2 = s^2 \sigma_{\mp}^2 (\rho_{\mp}^2 + 1) e^{2\Omega_R(s, t)} , \quad (20)$$

which does not describe well the forward scattering data. To improve we add to the real part a shape function

$$G_{\mp}^R(s, t) = \sigma_{\mp} \frac{s t}{\Lambda^2 - t} e^{\Omega_R(s, t)} , \quad (21)$$

which is zero for $t = 0$ and does not affect crossing symmetry. The amplitude is then written as

$$F_{\mp}^N(s, t) \rightarrow F_{\mp}^N(s, t) + G_{\mp}^R(s, t) . \quad (22)$$

The sum of the squared amplitudes is

$$\begin{aligned} |F_{\mp}^R(s, t)|^2 + |F_{\mp}^I(s, t)|^2 &\simeq s^2 \sigma_{\mp}^2 (\rho_{\mp}^2 + 1) e^{2\Omega_R(s, t)} \\ &+ 2 s \sigma_{\mp} G_{\mp}^R(s, t) (\rho_{\mp} \cos \Omega_I - \sin \Omega_I) e^{\Omega_R} + [G_{\mp}^R(s, t)]^2 . \end{aligned} \quad (23)$$

A more complete t dependence of $G_{\mp}^R(s, t)$ may also contain terms with negative parity, for example, the Odderon (for a review see [7]) which may be important for larger t values, specially at the dip region.

The real part is approximatly linear in t for small t and accounts for a zero with an energy dependence, which corresponds to Martin's zero [8], while in the imaginary amplitude there is no zero, since this model does not intend to describe the dip region. This can be seen due to the lack of the minus sign in the rotation matrix Eq.(17).

The derivatives of the logarithm of the real and imaginary amplitudes at

80 $|t| = 0$ are respectively,

$$\begin{aligned} \frac{\partial}{\partial t} \log F_{\mp}^R(s, t) \Big|_{|t|=0} &\simeq -\frac{1}{\rho_{\mp}} \frac{\partial \Omega_I(s, t)}{\partial t} \Big|_{|t|=0} + \frac{\partial \Omega_R(s, t)}{\partial t} \Big|_{|t|=0} \\ &+ \frac{\partial \log(G_{\mp}^R(s, t))}{\partial t} \Big|_{|t|=0} \equiv \frac{B_{\mp}^R(s)}{2} \end{aligned} \quad (24)$$

and

$$\frac{\partial}{\partial t} \log F_{\mp}^I(s, t) \Big|_{|t|=0} \simeq \rho_{\mp} \frac{\partial \Omega_I(s, t)}{\partial t} \Big|_{|t|=0} + \frac{\partial \Omega_R(s, t)}{\partial t} \Big|_{|t|=0} \equiv \frac{B_{\mp}^I(s)}{2}, \quad (25)$$

where B_{\mp}^R and B_{\mp}^I are referred to as the effective slopes of the real and imaginary amplitudes. These derivatives determine the average slope of the differential cross section at $|t| = 0$, which in terms of Eqs. (19), (24) and (25) is given by

$$B_{\mp}(s) \equiv \frac{d}{dt} \log \left(\frac{d\sigma_{\mp}}{dt} \right) \Big|_{|t|=0} = \frac{\rho_{\mp}^2 B_{\mp}^R + B_{\mp}^I}{\rho_{\mp}^2 + 1} = 2 \frac{\partial \Omega_R(s, t)}{\partial t} \Big|_{|t|=0} + \frac{\rho}{\rho^2 + 1} \frac{1}{\Lambda^2}. \quad (26)$$

85 The high energy behaviour ($\log^2 s$) of pp and $p\bar{p}$ total cross section implies $\rho \sim \pi / \log(s)$ for high energies [9], which compared with Eq.(19) automatically imposes $\beta = \pi/2$. The exact forms of dispersion relations can be computed for the amplitudes and their derivatives according to our recent mathematical results [10]. However, the energy dependence of the parameter η_3 needs to be
90 studied in detail.

We fix the parameters $P = 36$ mb, $P_1 = -1.5$ mb, $R_1 \cos(\eta_1 \beta) = 36.61$ mb, $R_2 \sin(\eta_2 \beta) = 26.15$ mb, $\eta_1 = 0.4473$ and $\eta_2 = 0.5486$, according to PDG parametrization (with some flexibility in the numerical values), living H as a free parameter. The parameters $b_0 = 11.36$ GeV⁻², $b_1 = 0.058$ GeV⁻², $b_2 = 0.0079$
95 GeV⁻² and $b_3 = -17.58$ GeV⁻² are fixed according to the global fit of all data analysed. The parameter β responsible for the crossing symmetry is stable in most of the studied energies and is compatible with $\pi/2$. We leave η_3 as a free parameter. We fit the experimental data from FNAL [11], ISR [12, 13], Sp \bar{p} S[14], E710[15] and LHC [16, 17, 18, 19, 20], covering a range of \sqrt{s} from
100 23 GeV to 13 TeV, using

$$\frac{d\sigma}{dt} = \frac{1}{16\pi(\hbar c)^2 s^2} |F(s, t)|^2, \quad (27)$$

where the amplitude $F(s, t)$ is

$$\frac{F(s, t)}{4\pi(\hbar c)^2 s} = \frac{F_{\mp}^N(s, t)}{4\pi(\hbar c)^2 s} + F_C(t) e^{i\Phi(s, t)} . \quad (28)$$

The Coulomb interaction together with the proton form factor is written for pp and p \bar{p} respectively

$$F_C(t) = \mp \frac{2\alpha}{t} \left(\frac{\Lambda^2}{\Lambda^2 - t} \right)^2 , \quad (29)$$

with $\alpha = 1/137$ (the fine structure constant) and $\Lambda^2 = 0.71 \text{ GeV}^2$ is the electromagnetic form factor scale. As discussed and justified in previous work [22] the Coulomb phase Φ is taken as zero.

COMPARISON WITH DATA

The datasets have been analysed in limited t -range ($0 < |t| < 0.2$) GeV^2 chosen appropriately for each dataset of them in order to account for the stability of β , which in our analysis is manifestly positive. The positiveness of the real amplitude for $|t|$ near zero was recently proved by A. Martin and T. T. Wu [23] and this supports our results for β .

We obtain that all datasets analysed are well represented by our model with reasonable small χ^2/ndf . The fits show that β is compatible with $\pi/2$ for all datasets. This parameter is related with the phase of the complex nuclear amplitude. Thus, if we consider $\beta = \pi/2$ as an input in Eq.(8) the scattering amplitude becomes crossing symmetric under $s \rightarrow u$ for fixed $-t$.

The energy dependence of $\eta_3(s)$, shown in the RHS of Fig.1, can be parametrized with a power of s as

$$\eta_3(s) = \epsilon_0 + \epsilon_1 s^{-\zeta} , \quad (30)$$

with the parameters $\epsilon_0 = 0.0568 \pm 0.0004$, $\epsilon_1 = 0.336 \pm 0.006$ and $\zeta = 0.182 \pm 0.003$. These parameters seem to be constant with energy, supporting the idea of the existence of a complex scaling function $f(\tau')$. The regular dependence of $\eta_3(s)$ is remarkable, and for very large energies this quantity tends to stay constant around $\epsilon = 0.056$.

125 In Table 1 we show the obtained parameters H , η_3 for all analysed energies and the extracted forward quantities σ , ρ , B , σ_{elas} . We also show predictions for the energies 0.2, 0.9, 2.76, 14 and 57 TeV.

An important feature of the model is Martin's zero in the real part of pp and $p\bar{p}$ [8]. Setting Eq.(15) equals zero we obtain the solution for Martin's zero.
 130 However, since we are working in very small $-t$ the trigonometric and the shape functions can be expanded in powers of t . We take the leading terms in the real amplitude and we write the position of the zero

$$|t_R| \simeq \frac{\rho_{\mp}(s)}{\beta [b_1 + 2 b_2 \log(s)] - b_3 s^{-\eta_3(s)} \sin[\eta_3(s)\beta] + 1/\Lambda^2} . \quad (31)$$

The RHS of Fig.1 shows the zeros of Martin for pp and $p\bar{p}$. For ISR energies the position of the zero moves to higher $-t$, but at TeV energies it starts to
 135 decrease as predicted by the theorem of Martin[8].

Fig.2 shows the amplitudes for pp and $p\bar{p}$ at similar energies about (52 GeV). The real parts are positive at $-t = 0$ and have zeros near the origin. The magnitude of the imaginary part is much larger than the real part for low $-t$ values.

140 Fig.3 shows the ratio $(d\sigma/dt - \pi(\hbar c^2)|F_{\mp}^I|^2)/(\pi(\hbar c)^2|F_{\mp}^I|^2)$ for $\sqrt{s} = 23, 44, 52, 62, 540, 1800$ GeV for both pp and $p\bar{p}$. This ratio removes from the differential cross section the simple exponential behaviour, which is essentially dictated by the imaginary part, allowing to investigate with detail the structure of the real amplitude. We observe that the curvature at all energies is created
 145 by the zero of the real part together with and the magnitude of the real slope.

The LHS of Fig. 4 shows the ratio $(d\sigma/dt - \pi(\hbar c^2)|F_{\mp}^I|^2)/(\pi(\hbar c)^2|F_{\mp}^I|^2)$ for LHC energies $\sqrt{s} = 7, 8$ and 13 TeV. As in the previous figures involving the data we add factors multiples of 0.05 to separate the data. For these LHC energies we note that a 'soft peak' structure is presented in the very forward
 150 region. In the RHS figure we show the real and imaginary amplitudes at 13 TeV, but this time we include the Coulomb amplitude. For pp scattering the Coulomb amplitude is negative while the real nuclear part is positive. The interplay between them produces a zero in the very forward range which can be

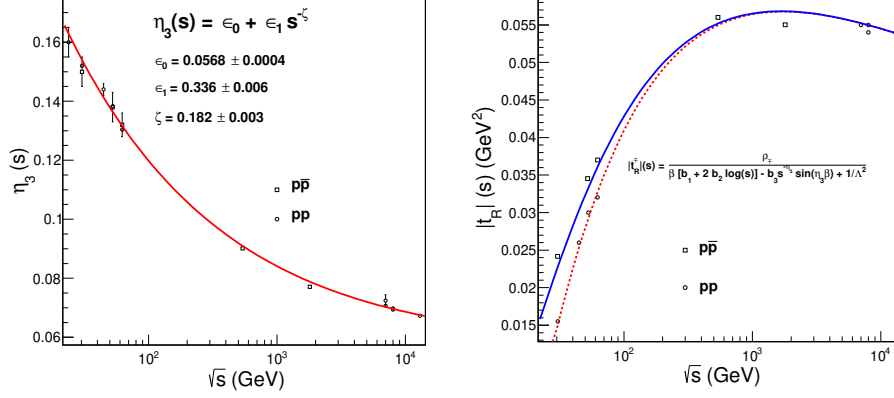


Figure 1: The LHS plot shows the energy dependence of the parameter η_3 . For high energies (LHC and beyond) the value of the parameter tends to stay constant around ϵ_0 . The RHS figure shows the zero of Martin for the real part obtained from our model. The symbols represent the zeros obtained from the fits. The curves are obtained with $\eta_3(s)$ and $|t_R|(s)$ from Eqs.(30) and(31).

seen in the figure.

155 The difficulties in the determination of the parameter ρ from the data are well known for various phenomenological models. A proper determination depends on the analytical form used to parametrize the nuclear interaction and on the interference with the Coulomb interaction which is still an open problem. The quality of the experimental data in the interference region is crucial for
160 this purpose. In the present model the analytical connection between the real and imaginary parts controls the fit instabilities, constraining ρ from dispersion relations. In this sense we understand that the Odderon term is not necessary to explain the LHC forward data. Other analysis also consider only the even (Pomeron) term to explain the forward data [21].

165 In recent studies of the LHC data on pp elastic scattering with independent real and imaginary amplitudes [22], specific features of the real part, such as the position of the zero and the magnitude and sign of the amplitudes were investigated, and the parameters were determined with high precision. In the present work we discuss properties of analyticity and crossing symmetry of the

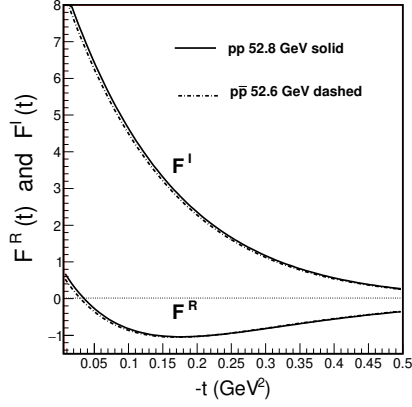


Figure 2: The figure shows the real and imaginary amplitudes for pp and $p\bar{p}$ at $\sqrt{s} = 52$ GeV. The real part has a zero close to $|t| \sim 0.034$ GeV². It is important to stress that these amplitudes are realistic until $-t \simeq 0.2$ GeV². Beyond this range, other terms might be necessary in the real and imaginary parts. In this figure we only consider nuclear part.

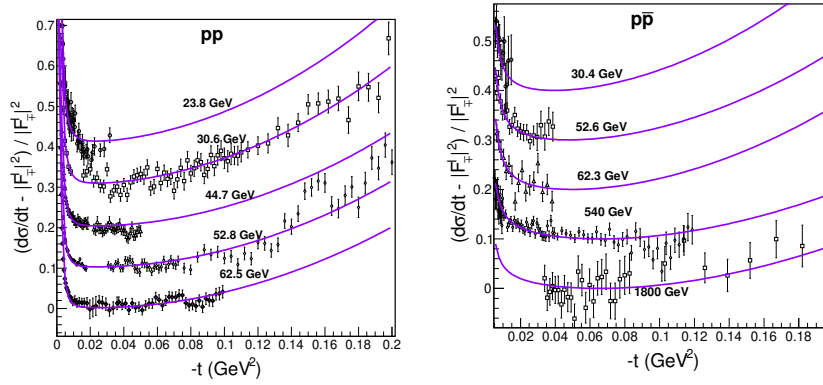


Figure 3: The LHS plot shows the quantity $(d\sigma/dt - \pi(\hbar c^2)|F_{\mp}^I|^2) / (\pi(\hbar c)^2|F_{\mp}^I|^2)$ for pp at ISR energies. The subtraction of the squared of the imaginary part essentially removes the pure exponential dependence of the differential cross section, putting in evidence the non-exponential behaviour of the distributions. To avoid the piling of the data at different energies we add to the y axis multiples of 0.1. The RHS plot is similar, for $p\bar{p}$ data from ISR/CERN and E710/Fermilab. Again we add to the curves and the data multiples of 0.1.

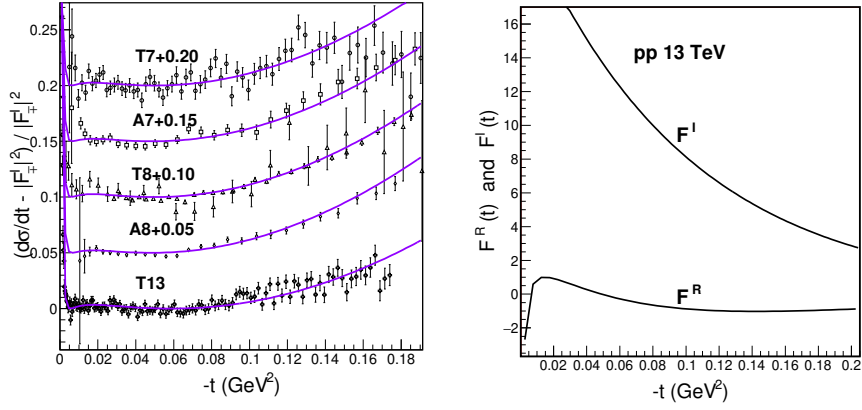


Figure 4: The LHS plot shows $(d\sigma/dt - \pi(\hbar c)^2|F_{\mp}^I|^2)/(\pi(\hbar c)^2|F_{\mp}^I|^2)$ at LHC energies. As before we add multiples of 0.1 in the curves and data to separate them. Note that at these energies a 'soft peak' is presented near $|t| = 0.006$ GeV². The RHS plot shows the real and imaginary amplitudes at 13 TeV together with the Coulomb interaction. Since the Coulomb amplitude is negative for pp and the real nuclear part is positive for small $-t$ there is a region where their sum cancels out, producing a minimum. This effect explains the peak that could be present for very forward scattering at high energies.

170 amplitudes in the forward regime. It is important to remark that the real and
imaginary amplitudes Eq.(17), when expanded to small $-t$ values, have similar
forms on t compared with the amplitudes in previous work [22]. The main
difference is in the imaginary part of [22] which contains an additional linear
factor on t that accounts for the existence of the dip in the differential cross
175 section for larger t values. This difference influences the parameters of the real
part giving small modifications in the quantities such as t_R and the effective
slope B_R^{eff} .

Advocated in [2], the geometric scaling is reached when the s and t de-
pendence can be written in terms of a single variable $\tau(s, t)$. At this regime
180 of very high energies the real part should vanish and the scattering ampli-
tude should be dominated by the imaginary part. In our case the real am-
plitude is still very important in the current LHC energies. However, for
very high energies the geometric scaling due to the imaginary part is given
by $F_I(s, t)/F_I(s, 0) \simeq \exp(\Omega_R(\tau'))$.

185 Acknowledgments

The ideas of this work emerged from discussions in the EDS Blois 2017 Con-
ference in Prague, particularly with Profs. André Martin and Otto Nachtmann.
The author thanks Profs. Erasmo Ferreira and Takeshi Kodama for useful dis-
cussions and for stimulating this work and reading of the manuscript. The
190 author also thanks the Brazilian agency CAPES for financial support.

References

References

- [1] M Froissart, Phys. Rev. **123** (1961) 1053.
- [2] G. Auberson, T. Kinoshita and A. Martin, Phys. Rev. D **3** (1971) 12; J.
Dias De Deus, Nuc. Phys. B **59** (1973) 231; I. Bautista and J. Dias De
195 Deus, Phys. Lett. B **718** (2013) 1571.

- [3] A. Martin, Lett. Nuovo Cim. **7** (1973) 811.
- [4] D. Fagundes and M. Menon, Int. J. Mod. Phys. A **26** (2011) 3219.
- [5] M. M. Block and R. N. Cahn, Rev. Mod. Phys **57** (1985) 563.
- 200 [6] COMPETE Collaboration, Phys. Rev. Lett. **89**, 201801
- [7] C. Ewerz, hep-ph/0306137 (2003).
- [8] A. Martin, Phys. Lett. B **404** (1997) 137.
- [9] N. N. Khuri and T. Kinoshita, Phys. Rev. B **137** (1965) 720.
- [10] E. Ferreira and J. Sesma, J. Math. Phys. **49** (2008) 033504; E. Ferreira and
 205 J. Sesma, J. Math. Phys. **54** (2013) 033507; E. Ferreira, A. K. Kohara and
 J. Sesma, Phys. Rev. D **98** (2018) 094029;
- [11] A. A. Kuznetsov et al. , Sov. J. Nucl. Phys. **33**, (1981) 74, and Yad. Fiz.
33, (1981) 142.
- [12] U. Amaldi and K.R. Schubert, Nucl. Phys. B **166**, (1980) 301.
- 210 [13] N. Amos, et al., Nuc. Phys. B **262** (1985) 689.
- [14] C. Augier et al. , [UA4/2 Coll.] , Phys. Lett. B **316**, (1993) 448.
- [15] Amos et al. [E-710 Coll.], Phys. Lett. **B** 247, (1990) 127.
- [16] G. Aad et al. [ATLAS Coll.], Nucl. Phys. B **889** (2014) 486.
- [17] G. Aad et al. [ATLAS Coll.], Phys. Lett. B **761** (2016) 158.
- 215 [18] G. Antchev et al. [TOTEM Coll.], Eurphys. Lett. **101** (2013) 21002.
- [19] G. Antchev et al. [TOTEM Coll.], Eur. Phys. J. C. **16** (2016) 661; Nucl.
 Phys. B **899** (2015) 527.
- [20] G. Antchev et al., CERN-EP-2017-335.
- [21] A. Donnachie and P. V. Landshoff, arXiv:1904.11218 (2019).

- ²²⁰ [22] A. K. Kohara, E. Ferreira, T. Kodama and M. Rangel, Eur. Phys. J. C **77** (2017) 877; A. K. Kohara, E. Ferreira, T. Kodama and M. Rangel, Phys. Lett. B **789** (2019) 1.
- [23] A. Martin and T. T. Wu, arXiv:1708.08372.

parameters			derived quantities				χ^2/ndf	Refs
\sqrt{s} (GeV)	H (mb)	η_3	σ (mb)	ρ	B (GeV ⁻²)	$\sigma_{\text{elas.}}$ (mb)		
pp								
23.882	0.311±0.002	0.16 (fix)	39.57	0.034	11.77	7.27	90.7/62	[11]
30.6	0.292±0.001	0.1522±0.001	39.79	0.049	12.23	7.03	94.1/68	[12]
44.7	0.291±0.0004	0.144 (fix)	41.51	0.077	13.12	7.08	87.3/67	[12]
52.8	0.2894±0.0003	0.1383±0.0003	42.41	0.088	13.26	7.30	245/88	[12]
62.5	0.2812±0.0005	0.1304±0.0004	42.76	0.092	13.15	7.49	111.1/62	[12]
200*	0.2887 (fix)	0.106 (fix)	52.05	0.133	14.61	9.94	-	
900*	0.2887 (fix)	0.085 (fix)	68.38	0.145	16.43	15.15	-	
2760*	0.2887 (fix)	0.076 (fix)	84.04	0.143	18.23	20.51	-	
7000	0.2895±0.0003	0.0735±0.0002	99.51	0.138	20.39	25.57	74.4/59	[18]
7000	0.2764±0.0002	0.0707±0.0001	95.43	0.136	19.90	24.11	42.9/33	[16]
8000	0.2903±0.0001	0.0694±0.0001	102.12	0.137	19.65	27.99	72.5/58	[19]
8000	0.2735±0.0001	0.0698±0.0001	96.74	0.135	20.11	24.51	28.8/25	[17]
13000	0.2913±0.0001	0.0673±0.0001	111.43	0.134	20.99	31.11	149.4/126	[20]
14000*	0.2887 (fix)	0.067 (fix)	112.65	0.132	21.13	31.15	-	
57000*	0.2887 (fix)	0.063 (fix)	141.59	0.123	24.19	42.93	-	
p \bar{p}								
30.4	0.2994±0.003	0.15 (fix)	41.32	0.076	12.05	7.73	22.4/25	[13]
52.6	0.2971±0.001	0.138 (fix)	43.44	0.102	13.24	7.69	29.9/27	[13]
62.3	0.2938±0.003	0.132 ±0.004	44.13	0.107	13.32	7.89	19.9/15	[13]
540	0.2930±0.0004	0.0901±0.0003	62.95	0.145	15.65	13.52	164.9/97	[14]
1800	0.2706±0.001	0.0771±0.0004	73.71	0.141	17.19	16.78	43.8/53	[15]

Table 1: The left part of the table shows the parameters obtained in each analysed energy. It is interesting to note that H is almost constant in all domain. The parameter η_3 tends to saturate at high energies, allowing the extrapolation for larger energies. The right part of the table shows the derived forward quantities. The values of σ , ρ and B are in accordance with the parameters given by the experimental papers. The (*) are predictions whose there no analyzable data.